Received: 3 June 2021 | Revised: 12 July 2021 | Accepted: 24 July 2021

DOI: 10.1002/er.7157

RESEARCH ARTICLE

INTERNATIONAL JOURNAL OF ENERGY RESEARCH WILEY

Numerical-analytical study of earth-air heat exchangers with complex geometries guided by constructal design

Bruna Rodrigues Nunes[1] | **Michel Kepes Rodrigues**[1] | **Luiz Alberto Oliveira Rocha**[2] | **Matthieu Labat**[3] | **Sylvie Lorente**[4] | **Elizaldo Domingues dos Santos**[1] | **Liércio André Isoldi**[1] | **Cesare Biserni**[5]

[1]Computational Modeling (PPGMC), Federal University of Rio Grande (FURG), Rio Grande, Brazil

[2]Mechanical Engineering, University of the Vale do Rio dos Sinos (UNISINOS), Porto Alegre, Brazil

[3]National Institute of Applied Sciences (INSA), Laboratory of Materials and Construction Durability (LMDC), University of Toulouse, Toulouse, France

[4]Department of Mechanical Engineering, Villanova University, Villanova, Pennsylvania, USA

[5]Department of Industrial Engineering (DIN), Alma Mater Studiorum - University of Bologna, Bologna, Italy

Correspondence
Cesare Biserni, Department of Industrial Engineering (DIN), Alma Mater Studiorum - University of Bologna, Bologna, Italy.
Email: cesare.biserni@unibo.it

Funding information
Conselho Nacional de Desenvolvimento Científico e Tecnológico, Grant/Award Number: 306024/2017-9 /306012/2017-0/ 307791/2019-0; Coordenação de Aperfeiçoamento de Pessoal de Nível Superior, Grant/Award Number: Ph 854-15; Fundação de Amparo à Pesquisa do Estado do Rio Grande do Sul, Grant/ Award Number: Edital 02/2017 - PqG - Process: 17/2551-000111; CAPES; Universita di Bologna

Summary

Significant advancements in developing earth-air heat exchanger models have been detected in the past several decades. It is worth mentioning that this type of device takes advantage of the Earth's constant temperature to cool or heat spaces in buildings so that the identification of its most appropriate geometric configurations to reduce energy consumption is still an actual challenge. In this context, the present paper is focused on the geometric evaluation of several earth-air heat exchangers arrangements according to the Constructal Design method. The performance indicators are the minimization of its soil volume occupation, the minimization of its airflow pressure drop, and the maximization of its thermal potential. Therefore, from a straight duct named Reference Installation, 26 complex geometries have been outlined here using the numerical-analytical investigation. Many ideas emerged from this study: the use of serpentine with low spacing between ducts reduced nearly 39% of the soil volume occupied by the device compared to Reference Installation, showing its applicability in urban regions. In addition, configurations with few curves benefited the decrease of air pressure drop, allowing a performance 30% superior to the most complex shapes. Instead, complex designs can be recommended for thermal potential increase, although the influence of the different configurations over this indicator was not substantial since the maximum improvement achieved between the best and worst shapes proved to be around 6%. Finally, when the three performance indicators are concomitantly considered, several complex geometries reached an overall performance superior to the Reference Installation.

KEYWORDS

complex geometric configurations, earth-air heat exchanger, pressure drop, soil volume, thermal potential

1 | INTRODUCTION

Modern engineering projects have to contemplate the scarcity of natural resources, seeking to improve the energy conversion and also its management with reference to the economic assessment. In this sense, the rational use of renewable sources to diversify the energy matrix in the world is an important issue.

For climatization in buildings, air conditioning units are often used to provide thermal comfort, but they generally require high power demand. Therefore, several efforts have been carried out to reduce electric energy consumption and improve the thermal quality of the air for human convenience inside buildings. In this context, the Earth-Air Heat Exchanger (EAHE) can be used as an alternative to traditional air conditioning equipment for climatization in order to reduce energy consumptions.

The EAHE is composed of one or more ducts buried in the ground, through which airflows usually by the action of fans. It takes advantage of the solar thermal energy stored in the surface layer of the soil. In other words, the EAHE main operating principle[1,2] is based on the heat transfer from soil to the air in cold periods and heat exchange from the air to the soil in hot periods during the year. In this context, many studies have been carried out to investigate the thermal behavior of soil in different periods of the day and year[3-7] and the thermal behavior of the device for different conditions of the soil, climate, and applications.[8-10] Concerning the performance of EAHE, several experimental and numerical works have been devoted to evaluate the thermal potential (*TP*), a significant performance indicator for EAHE design.[1,2,11-15] Moreover, it has been verified that the *TP* is highly influenced by parameters of the fluid flow in the ducts, thermophysical properties of the soil, local climate, and so on.

In addition to the thermal potential, the volume of soil occupied by the device (V_s) and the pressure drop of airflow (h) proved to be pivotal aspects to investigate the design of EAHE. More specifically, the latter is important to scale out the driven system with the lowest energy consumption possible. Consequently, ducts arrangement has a strong influence over the work rate performed by the driven system.[16] In turn, the soil volume occupied by the EAHE installation is important mainly in urban regions, where the soil dimensions are limited by residential, commercial, or even industrial buildings. In Reference 17, for example, the pressure drop was evaluated indirectly by means of the Coefficient of Performance (COP) and concerning the volume of soil investigation, a new EAHE configuration in spiral form was proposed.

Moreover, several studies have been focused on the thermal performance of EAHE under different climates. Fazlikhani et al[18] analyzed numerically the efficiency of EAHE for different climatic conditions that occur in Iran (hot-arid and cold climates of cities of Yazd and Hamadan, respectively), investigating the influence of inlet air temperatures, pipe lengths, and ground temperatures on the cooling and heating performance of EAHE. Again, with reference to Iran, Shojaee and Malek[19] evaluated the effectiveness of a four-duct EAHE by means a computational model developed in Fluent ambient, considering the climate of four localities: Tehram, Rasht, Ahvaz, and Hamadan. Recently, Rosa et al[20] investigated computationally the EAHE thermal behavior in the hot Mediterranean climate: a complex geometric configuration with seven interconnected parallel ducts was studied, with reference to the spacing between ducts, ducts diameter, and flowing air velocity. Into experimental framework, Elminshawy et al[21] investigated in laboratory scale the effect of three different compaction levels for the soil with distinct values of relative density, void ratio, and porosity over the thermal performance of EAHE. Uddin et al[22] examined the thermal comfort performance of indoor air contemplating the life cycle energy and Greenhouse Gas (GHG) emissions. Bisoniya et al[23] presented a numerical evaluation of the annual heating and cooling potential of EAHE in India analyzing the economic assessment in terms of the energy payback time, CO_2 emission mitigation potential, and carbon credit earned. More recently, Victoria et al[24] proposed a methodology for numerical simulations of EAHE which ally Standard Penetration Test (SPT) reports to determine soil stratification with the air and soil surface temperatures variations from ERA-Interim data. This methodology can be adopted to analyze the EAHE performance anywhere in the World, as in Reference 25 it was utilized for the thermal behavior of a device installed in the coastal city of Rio Grande, southern Brazil, which has a humid temperate climate.

Several works have also been focused on EAHE design methodologies. Paludetto and Lorente[26] introduced a novel approach for the design of an underground heat exchanger connecting a datacenter (the heat source) to office buildings (the heat sinks). Moreover, Rodrigues et al[1] and Brum et al[27] investigated, in accordance with Constructal Design, several configurations for the arrangement of parallel straight pipes (pair, triangular, rectangular, and diamond). Constructal Design method[28-32] is based on balancing constraints and degrees of freedom for evaluation of any animate or inanimate finite size flow systems. Constructal theory proved to be fully versatile and interdisciplinary, as it was used to demonstrate that even natural systems follow a physical principle of generation, configuration, and design evolution. It is worth mentioning that Constructal Design method has been applied, with

reference to its original focus, for evaluation of shape and structure in many engineering problems as heat transfer, renewable energy, and even solid mechanics.[1,27,33-35] Recently, Estrada et al[34] focused on the impact of latent heat exchange over the EAHE system overall performance in continental and tropical climates. The geometrical optimization was performed by means of Constructal Design. However, none of the above-mentioned works are concerned with the geometrical evaluation of complex EAHE devices considering a multi-objective approach.

In the context of growing literature regarding EAHE design optimization,[36-41] the present paper is aimed to fill this gap by contemplating simultaneously, in coherence with Constructal Design, the following performance indicators: (a) minimization of the required soil volume for the EAHE system, (b) minimization of the EAHE pressure drop and (c) maximization of the EAHE thermal potential. The main goal is the investigation of several complex configurations of EAHE, with changes being performed according to Constructal Design from a reference installation case, analyzing the problem in a multiobjective viewpoint and seeking to minimize the occupation volume of soil, which is important for the design of EAHE in urban areas, but without causing a significant increase in pressure drop and a significant decrease in thermal potential. To the best of the author's knowledge, this kind of investigation with an application of Constructal Design for complex configurations and investigating various performance parameters were not previously studied in the literature. More specifically, 26 different EAHE installations with complex geometries are compared based on these three parameters. The main restriction here imposed is the duct length which remains unchanged in all configurations, that is, the overall volume of airflow is constant. The reason is that the length scale comes from a reference case where a rectilinear duct is buried in a fixed portion of the soil. The depth of the soil, the depth of EAHE installation and the duct diameter are also fixed, being constraints according to the problem statement of Constructal design here developed. Finally, it is worth mentioning that the numerical modeling here used has been previously validated by means of comparison with the experimental results presented in Reference 11.

2 | PROBLEM STATEMENT

2.1 | EAHE reference installation (RI)

In the present work, the soil volume necessary for the EAHE installation is taken from the soil volume used in a reference installation, which consists on a straight duct buried in the soil.

Figure 1A shows a schematic view of the computational domain with the boundary conditions of RI and Figure 1B depicts a view of the *x-y* cross-sectional plan (see gray surface in Figure 1A) with dimensions. The driven flow is caused by the imposition of constant velocity profile of air with $v_{in} = 3.3$ m/s in the inlet of the duct domain. Moreover, a manometric pressure is imposed at the exit ($p_{out} = 0$ Pa) and in the ducts walls it is imposed a non-slip and impermeability boundary conditions. Concerning the thermal boundary conditions, the lateral, and lower surfaces of the soil are thermally insulated, in coherence with References 1, 11, 12.

Still regarding Figure 1A, in the duct inlet and upper soil surface, different prescribed temperatures are imposed as a function of time for the air, $T_{in}(t)$, and for the soil surface, $T_{sur}(t)$, being respectively given by (in°C):

$$T_{in}(t) = 23.18 + 6.92 \cdot \sin\left(1.72 \times 10^{-2} \cdot t + 26.42\right), \quad (1)$$

$$T_{sur}(t) = 18.70 + 6.28 \cdot \sin\left(1.72 \times 10^{-2} \cdot t + 26.24\right), \quad (2)$$

where t is the $T_P(t) = 23.18 + 6.92\sin(0.0172t + 26.42)$ time (s).

For achievement of Equations (1) and (2), experimental data illustrated in Reference 11 were statistically adjusted using the least squares method.[1,11] The imposed boundary conditions are in coherence with the conditions monitored by Vaz et al[11] in the southern city of Viamão (Brazil), where the climate is temperate with winter and summer well defined. Posteriorly, in the work of Brum et al[12] a computational model was developed and several recommendations about the transient soil temperature and EAHE behavior for different installation depths were presented. Therefore, based on these two previous works, the boundary conditions used in the present work were consequently defined.

In the computational approach, the wall thickness of the duct has been neglected. In the model, it was supposed that airflows through cylindrical perforations inserted directly into the soil volume. Two main reasons justify the use of this simplification:

- the first one is related with the required high degree of mesh refinement when the thickness is considered, since the thickness dimension is high orders lower than the soil domain;
- the second one is concerned with the conductive thermal resistance of the duct which is strongly lower than thermal resistance in the air duct flow and soil. This assumption does not significantly alter the final solution of the problem and has been adopted in previous studies.[1,11,12,27,42,43]

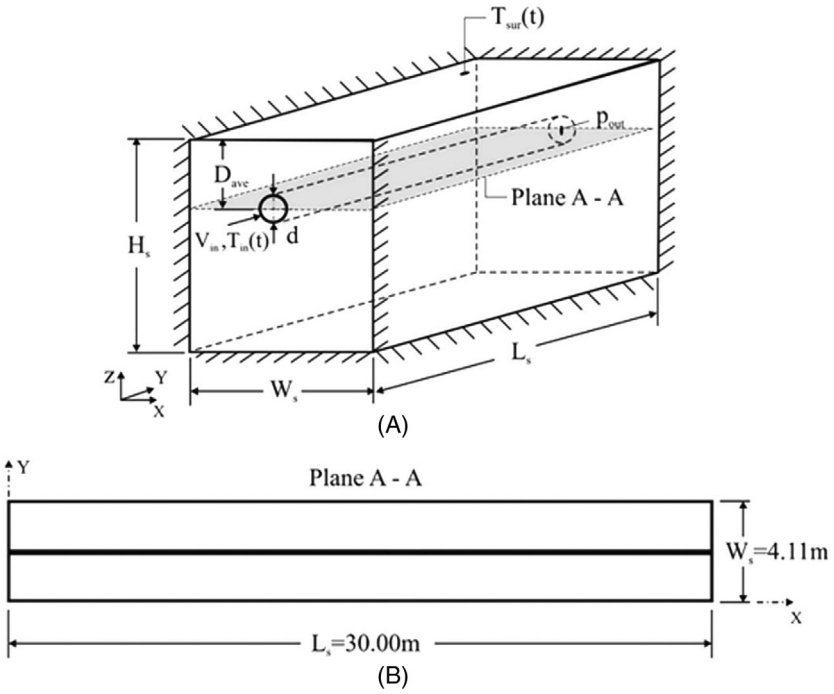

FIGURE 1 Computational domain and boundary conditions of the EAHE model: A, schematic perspective view, B, top view (Plane A-A) with dimensions of Reference Installation (RI)

TABLE 1 Thermo-physical properties of the materials[11,12]

Property material	Density (kg/m^3)	Thermal conductivity (W/m·K)	Specific heat (J/kg·K)	Absolute viscosity (kg/m·s)
Air	1.16	0.0242	1010	1.798×10^{-5}
Soil	1800	2.1	1780	-

Thermo-physical properties of air and surrounding clay soil were experimentally determined and indicated in References 11, 12, as reported in Table 1.

Concerning the domain dimensions, ducts are buried at the average depth of $D_{ave} = 3.00$ m in relation to the superior soil surface. This depth was selected according to previous theoretical recommendations illustrated in Reference 12, where it was noticed that exceeding this depth there is no more significant gain in thermal potential of EAHE for the same thermal conditions here investigated. Moreover, the duct has an internal diameter of $d = 110$ mm and the total length is $L = 30.00$ m for all installations here proposed, in coherence with References 1, 11, 12.

2.2 | Volume of soil occupied by EAHE installations

The present problem is subjected to the installation volume of soil (V_s), which is given by:

$$V_s = L_s \cdot W_s \cdot H_s, \tag{3}$$

where: $H_s = 15.00$ m for all the cases since there is no significant variation in the mean soil temperature from that depth.[11,12] For the RI case, the dimensions of the soil are given also by $L_s = 30.00$ m and $W_s = 4.11$ m (see Figure 1A,B).

Once different volumes of soil (V_s) which circumscribes the ducts arrangements are investigated with the purpose to minimize its dimensions, the soil volume is defined in a normalized way:

$$V_N = \frac{V_s}{V_{RI}}, \tag{4}$$

where V_{RI} is the soil volume occupied by the RI.

For all design configurations here studied, it is considered a horizontal spacing between the wall of the duct and the wall of the computational domain of $S_w = 2.00$ m. This value represents the inferior limit where the prescribed null heat flux imposed in lateral surfaces of the soil does not cause interference in the thermal distribution in the ducts.[44] Horizontal spacing between the walls of two parallel ducts lower than $S = 1.00$ m is also considered. This value is taken from

Reference 44, where it was observed that for $S < 1.00$ m there is a significant influence on the heat exchange between the duct and soil in comparison with a solely duct, resulting in a reduction of the *TP* of EAHE. Therefore, in this study values for spacing between ducts of $S = 1.00$ m, 2.00 m, 3.00 m, and 4.00 m were defined and adopted for the geometric constructions.

2.3 | Air pressure drop in EAHE installations

For internal flows, the distributed and localized pressure drop can be calculated analytically according to References 45, 46. Therefore, in fully developed turbulent flow, the distributed pressure drop (h_d) can be approximated as follows:

$$h_d = f \cdot \frac{L}{d} \cdot \frac{v^2}{2g}, \tag{5}$$

where L is the total linear length of the duct network (m); v is air velocity (m/s), d is duct diameter (m), g is the gravitational acceleration (9.81 m/s^2) and f is the friction factor, dependent of the Reynolds number (Re_d) and the duct relative roughness (ε/d).

To avoid inaccuracy of the graphical method for determining f under fully developed turbulent flow in circular ducts, based on Moody's data, it can be used a correlation given by References 45, 46:

$$\frac{1}{\sqrt{f}} = -2.0\log\left(\frac{\varepsilon/d}{3.7} + \frac{2.51}{\mathrm{Re}_d\sqrt{f}}\right). \tag{6}$$

However, Equation (6) is implicit in f. As an alternative to determine f value explicitly for $\mathrm{Re}_d \geq 3000$ it can be used another expression given by References 45, 47:

$$f = \left\{-1.8\log\left[\left(\frac{\varepsilon/d}{3.7}\right)^{1.11} + \frac{6.9}{\mathrm{Re}_d}\right]\right\}^{-2}. \tag{7}$$

Having fixed $d = 110$ mm, $\varepsilon = 0.05$ mm and $\mathrm{Re}_d = 23\,419.35$, the value of $f = 0.026$ is the result of Equation (7). It is worth mentioning that the maximum percentage deviation in results between Equation (7) and (6) is 2%.

Moreover, in internal flows, localized pressure drop (h_l) is commonly computed as follows[45,46]:

$$h_l = K_l \cdot \frac{v^2}{2g}, \tag{8}$$

where: K_l is the device loss coefficient, being defined based on References 45, 46.

Finally, the air pressure drop in the EAHE (h) is the sum of the air distributed pressure drops (h_d) with the air localized pressure drops (h_l), resulting in:

$$h = h_d + h_l. \tag{9}$$

It is worth mentioning that the airflow pressure drop in the EAHE is a fundamental parameter for the determination/selection of the fan power required for the system. Here, a normalized air pressure drop (h_N) is considered, being defined as:

$$h_N = \frac{h}{h_{RI}}, \tag{10}$$

where h_{RI} is the air pressure drop of the RI.

2.4 | Thermal potential of the EAHE installations

The Thermal Potential (*TP*) is a pivotal indicator to evaluate the thermal performance of the EAHE and can be determined from an annual averaged air temperature. The *TP* of the EAHE installation can be expressed as follows[1,12]:

$$TP = \sqrt{\frac{\sum_{i=1}^{1460}\left(T(t)_i^{out} - T(t)_i^{in}\right)^2}{1460}}, \tag{11}$$

where: $T(t)^{out}$ is the transient air temperature (in °C) at the duct outlet, $T(t)^{in}$ is the transient air temperature (°C) at the duct inlet (prescribed temperature condition) and i varies from 1 to 1460, representing the outlet temperature measurements performed every 21 600 seconds during the second year of the numerical simulation. Therefore, when $T(t)^{out} > T(t)^{in}$ the airflow is being heated; when $T(t)^{out} < T(t)^{in}$ the airflow is being cooled and when $T(t)^{out} = T(t)^{in}$ there is no heat transfer between the soil and aiflow.

The thermal potential is also evaluated in its normalized form (TP_N):

$$TP_N = \frac{TP}{TP_{RI}}, \tag{12}$$

where: TP_{RI} is thermal potential of the RI configuration.

However, there are no generalized analytical methods to determine the *TP* for the different EAHE installations.

Thus, for the evaluation of thermal potential, it is necessary to solve the thermal field by means of numerical approach. Here, the conservation equations of mass, momentum, and energy are solved by means of a Computational Fluid Dynamics (CFD) package, FLUENT (version 14.0), based on Finite Volume Method (FVM).[48-50] Therefore, computational simulations are performed to determine $T(t)^{out}$ values.

3 | MATHEMATICAL AND NUMERICAL MODELING

For the evaluation of the transient temperature field in the soil, it is solved the energy equation, given by[51,52]:

$$\frac{\partial T}{\partial t}=\frac{\partial}{\partial x_j}\left\{\alpha_s\frac{\partial T}{\partial x_j}\right\}\ (j=1,2,\text{and } 3), \tag{13}$$

where: α_s is soil thermal diffusivity (m^2/s), T is soil temperatures field (K), t is the time (s), x_j represents the spatial coordinates ($j = 1$, 2 and 3) (m).

For the modeling of transient, incompressible, and turbulent forced convective flows in the duct of the EAHE, the conservation equations of mass, momentum, and energy, respectively, are given expressed as follows, in coherence with References 51, 53, 54:

$$\frac{\partial \overline{v_i}}{\partial x_i}=0\ (i=1,2,\text{and } 3), \tag{14}$$

$$\frac{\partial \overline{v_i}}{\partial t}+\frac{\partial\left(\overline{v_i}\,\overline{v_j}\right)}{\partial xj}=-\frac{1}{\overline{\rho}}\frac{\partial \overline{p}}{\partial x_j}\delta_{ij}+\frac{\partial}{\partial x_j}\left\{\upsilon\left(\frac{\partial \overline{v_i}}{\partial x_j}+\frac{\partial \overline{v_j}}{\partial x_i}\right)-\tau_{ij}\right\}\ (i,j=1,2,\text{and } 3), \tag{15}$$

$$\frac{\partial \overline{T}}{\partial t}+\frac{\partial}{\partial x_j}\left(\overline{v_j T}\right)=\frac{\partial}{\partial x_j}\left\{\alpha\frac{\partial \overline{T}}{\partial x_j}-q_j\right\}\ (j=1,2,\text{and } 3), \tag{16}$$

where the overline represents the time-averaged terms, x_i are the spatial coordinates ($i = 1$, 2, and 3) (m), v_i are the velocity in Cartesian directions ($i = 1$, 2, and 3) (m/s), δ_{ij} is the Kronecker delta, p represents the pressure (Pa), υ is the kinematic viscosity of the air (m^2/s) and α is the thermal diffusivity of the air (m^2/s). The terms τ_{ij} and q_j that arise in the filtering process of the momentum and energy conservation equation, respectively, need to be modeled and can be written as[53,54]:

$$\tau_{ij}=\overline{v_i' v_j'}, \tag{17}$$

$$q_j=\overline{v_i' T_j'}, \tag{18}$$

where: the (′) indicates the time varying fluctuating component.

Regarding the closure problem, it is used the RANS k-ε model, which is based on the solution of two additional transport equations. For incompressible flows, the closure terms of Equations (17) and (18) are given by[53,54]:

$$\tau_{ij}=\upsilon_t\left(\frac{\partial \overline{v_i}}{\partial x_j}+\frac{\partial \overline{v_j}}{\partial x_i}\right)-\frac{2}{3}k\delta_{ij}, \tag{19}$$

$$q_j=\alpha_t\frac{\partial \overline{T}}{\partial x_j}, \tag{20}$$

where: υ_t is the kinematic eddy viscosity (m^2/s), k is the turbulent kinetic energy (m^2/s^2) and α_{sgs} is the thermal eddy diffusivity (m^2/s). The values of υ_t and α_t can be defined as:

$$\upsilon_t=C_\mu\frac{k^2}{\varepsilon}, \tag{21}$$

$$\alpha_t=\frac{\upsilon_t}{\mathrm{Pr}_t}. \tag{22}$$

The turbulent kinetic energy (k) and turbulent dissipation (ε) are, respectively, given by[54]:

$$\frac{\partial k}{\partial t}+\overline{v}_j\frac{\partial k}{\partial x_j}=\tau_{ij}\frac{\partial \overline{v}_i}{\partial x_j}+\frac{\partial}{\partial x_j}\left[\left(\upsilon+\frac{\upsilon_t}{\sigma_k}\right)\frac{\partial k}{\partial x_j}\right]-\varepsilon, \tag{23}$$

$$\frac{\partial \varepsilon}{\partial t}+\overline{v}_j\frac{\partial \varepsilon}{\partial x_j}=\frac{\partial}{\partial x_j}\left[\left(\upsilon+\frac{\upsilon_t}{\sigma_\varepsilon}\right)\frac{\partial \varepsilon}{\partial x_j}\right]+C_{\varepsilon 1}\frac{\varepsilon}{k}\tau_{ij}\frac{\partial \overline{v}_i}{\partial x_j}-C_{\varepsilon 2}\frac{\varepsilon^2}{k}, \tag{24}$$

being: $C_\mu = 0.09$, $C_{\varepsilon 1} = 1.44$, $C_{\varepsilon 2} = 1.92$, $\sigma_k = 1.00$, $\sigma_\varepsilon = 1.3$ and $\mathrm{Pr}_t = 1.00$. More details about the modeling of k-ε turbulence model can be found in literature.[53,54]

It is worth mentioning that in literature the Reynolds Stress Model (RSM) for turbulence closure is widely used (see eg, References 11, 12); despite this, in the present work we have consciously chosen to adopt the k-ε model. The main reasons are concerned with difficulties of suitable convergence of RSM model for some of the complex arrangements and the reduction of nearly 20% in processing time for simulations with k-ε model. Moreover, for the cases where both models have a suitable convergence, it is not observed significant variations between transient thermal fields.

Equations (13)-(16) and Equations (23) and (24) have been solved using the Finite Volume Method (FVM) implemented in the computational package FLUENT, version 14.0.[48-50]

The Upwind advection scheme is used for treatment of the advective terms and Coupled algorithm is adopted for treatment of the pressure-velocity scheme. Simulations are considered converged when the residues between two consecutive iterations are lower than 10^{-6}.

For the numerical simulations, a time step of 3.600 seconds (1 hour) is adopted in total of 17 520 time-steps, accumulating 2 years of simulation. However, only results obtained in the second year of simulation have been utilized and recounted. As in References 1, 11, 12, 27, the first simulation year has been dedicated to the adequate soil temperature stabilization. Therefore, the analysis ideally started at 00:00 hour on January 01, and ended at 00:00 hour on January 01, in coherence with References 11, 12. In addition, the initialization temperature of the computational model was 18.70°C (291.85 K), which represents the mean soil temperature (see Equation [2]).

The successive refinement technique is indicated to define the no-dependent mesh computational solution. Accordingly, it should be done an increase in the number of computational cells from the current mesh refinement to the next mesh refinement until to reach a relative difference between the thermal potential of two consecutive mesh refinements equal or less than 2.00×10^{-3}. This procedure is explained in detail in Reference 1 and for the sake of conciseness has not been here reproduced. However, it is worth mentioning that, based on this procedure, the spatial discretization of each EAHE installation numerically simulated in the present work has been performed by tetrahedral computational cells generated with a refinement of $d/3$ for the duct and $3d$ for the soil, being d the duct diameter.

3.1 | Validation and verification of the numerical model of EAHE

The results of an experimental study,[11,12] performed in the Viamão city, RS, Brazil (geographic coordinates: 30° 04′ 51″ S, 51° 01′ 24″ W and an altitude of 111 m), were used to validate the computational model used in this work. An EAHE with an irregular geometric configuration was considered in References 11, 12, being composed by three ducts: duct A (diameter of 110 mm and air inlet velocity of 3.3 m/s), duct B (diameter of 110 mm and air inlet velocity of 3.6 m/s), and duct C (diameter of 100 mm and air inlet velocity of 2.5 m/s).

For the computational model validation procedure, a simplified version of the above described EAHE was adopted, that is, only straight stretch sections of the ducts arrangement were considered. The computational configurations and thermo-physical properties are the same as those used in Reference 1, being the only exception the used turbulence model. Therefore, the numerical results are obtained from periodic measurements (for the annual temperature variation) by a numerical probe located at the outlet of the EAHE duct.

For the sake of brevity, in this work, the analysis is only promoted for the straight stretch of duct A. However, an analogous procedure with complete validation taking into accounts the ducts A, B, and C of References 11, 12 has been extensively reported in Reference 1.

Figure 2 shows the variation of the air outlet temperature of duct A as a function of time, allowing the comparison among the experimental data of Reference 11, 12, the numerical solution obtained by means of the RSM turbulence model illustrated in Reference 1 and numerical results of the present work (generated with the k-ε turbulence model). The outlet temperature curve was adjusted from the experimental data presented in References 11, 12 is given by:

$$T_{adj.out}(t) = 21.02 + 4.68 \cdot \sin\left(1.82 \times 10^{-2} \cdot t + 0.71\right), \quad (25)$$

where: $T_{adj.out}(t)$ is defined in°C and t is the $T_P(t) = 23.18 + 6.92\sin(0.0172t + 26.42)$ time (s).

Based on pure observation from Figure 2, the first relevant remark is that there is no significant difference between numerical results obtained with RSM turbulence model[1] and numerical results obtained with k-ε turbulence model (present work), being these solutions superimposed with a Pearson's R correlation coefficient of 0.999. Moreover, if the numerical results generated in the

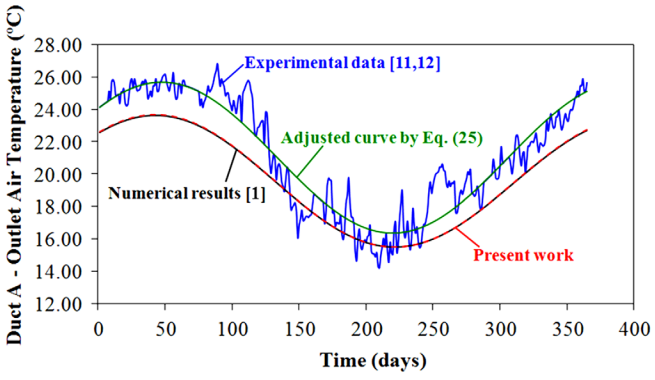

FIGURE 2 Validation and verification process of the numerical model of EAHE

present work are compared with the experimental data of,[11,12] it is found an absolute mean deviation around 1.60°C, representing an absolute mean error of 7.2%. In other words, the present numerical solution achieves a Pearson's R correlation coefficient of 0.946 if compared with the experimental data adjusted by Equation (25). As a consequence, it is assumed that, in spite of slight differences in comparison with results of literature, the present model results to be fully verified and validated.

4 | COMPLEX DESIGN CONFIGURATIONS PROPOSED FOR THE EAHE

In this study, the conventional EAHE with a straight duct is named Reference Installation (RI), being considered the elementary construction (see Figure 1A,B).

Starting from the RI, with the soil volume occupied $V_s = 1849.50\ m^3$, and keeping constant the duct length, 26 installations of EAHE with complex geometric configuration were defined and numerically investigated in the present work. The complex geometries are composed with straight stretches of ducts connected by at least one curve (with 90° or 180°).

For all EAHE installations here studied, the following dimensions and parameters are used: $d = 110$ mm, $L = 30.00$ m, $D_{ave} = 3.00$ m, $S_w = 2.00$ m, $H_s = 15.00$ m, Reynolds number of $Re_d = 23\ 531.91$, Prandtl number of Pr = 0.70 and volumetric flow rate of air inside the duct of $\dot{V} = 3.14 \times 10^{-2}\ m^3/s$.

In order to facilitate the discussion of results with reference to many scenarios, the complex geometric configurations have been organized into five groups. In each group, installations are arranged to have at least one common geometric element (curves of 90° or 180°). With the purpose to illustrate the designs, the complex EAHE installations are presented from an upper view analogous to that showed in Figure 1B, indicating the airflow direction, and the main dimensions of each configuration.

Figure 3 illustrates the EAHE designs of Group 1, which consists on five different installations and it is identified by increasing the number (n) of the curves with 180°. More precisely, the EAHE installations I1, I2, I3, I4, and I5 are constituted, respectively, by $n = 2$; 3; 4; 5 and 6 curves of 180°. Moreover, the spacing between ducts is $S = 1.00$ m for all installations of Group 1. Soil volumes defined for occupancy of the EAHE installations I1, I2, I3, I4, and I5 are equal to $V_s = 1169.78\ m^3$; $1128.28\ m^3$; $1126.04\ m^3$; $1144.71\ m^3$, and $1174.47\ m^3$, respectively.

Figure 4 shows schematic upper views of the EAHE configurations with reference to Group 2, which is composed by five installations classified according to 90° curves number and 180° curves number. In this way, it can be seen that Group 2 installations have $n = 2$ curves of 90° and $n = 2$; 3; 4; 5 and six curves of 180° for the

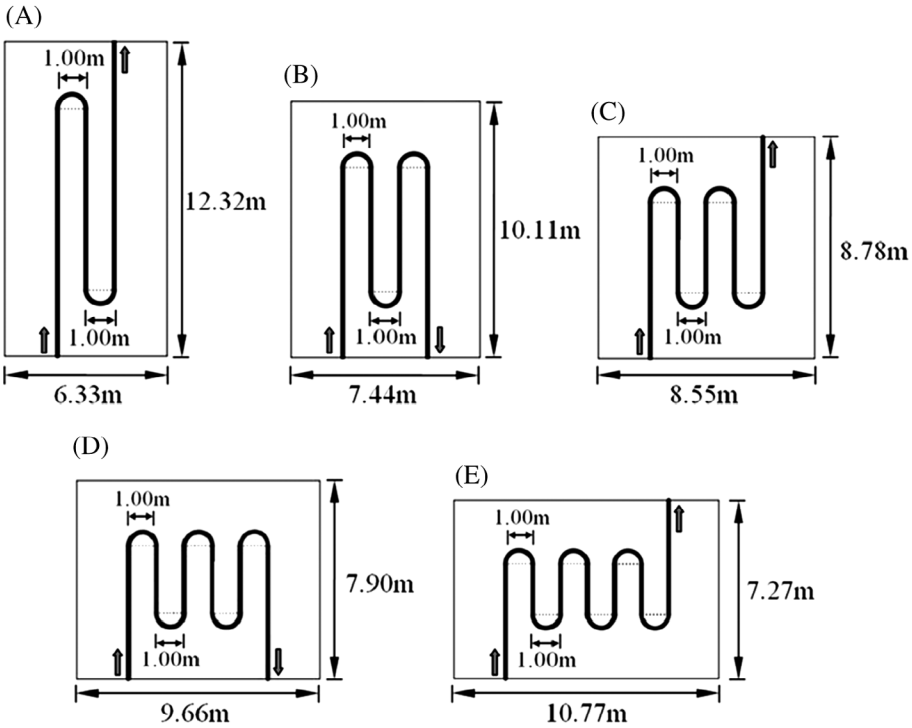

FIGURE 3 Configurations of the EAHE of the Group 1: A, Installation 1 (I1), B, Installation 2 (I2), C, Installation 3 (I3), D, Installation 4 (I4) and E, Installation 5 (I5)

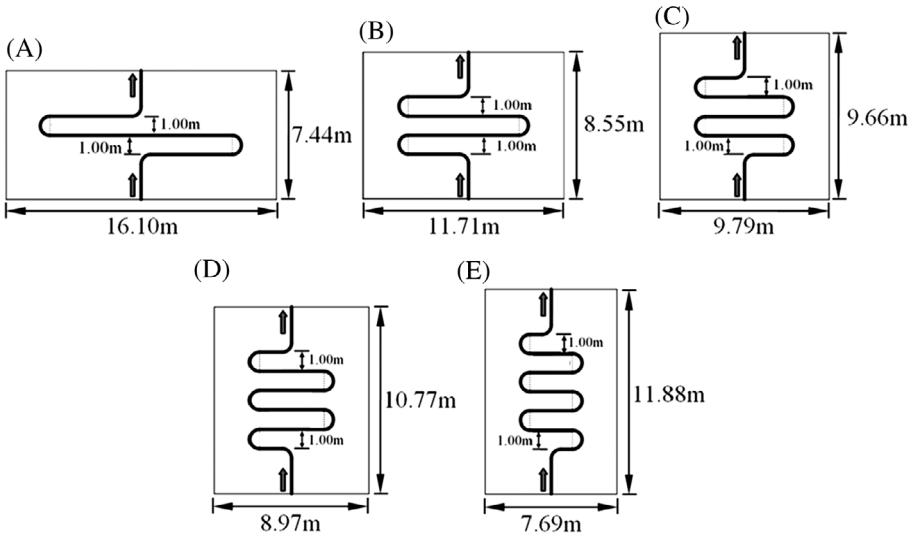

FIGURE 4 Configurations of the EAHE of the Group 2: A, Installation 6 (I6), B, Installation 7 (I7), C, Installation 8 (I8), D, Installation 9 (I9) and E, Installation 10 (I10)

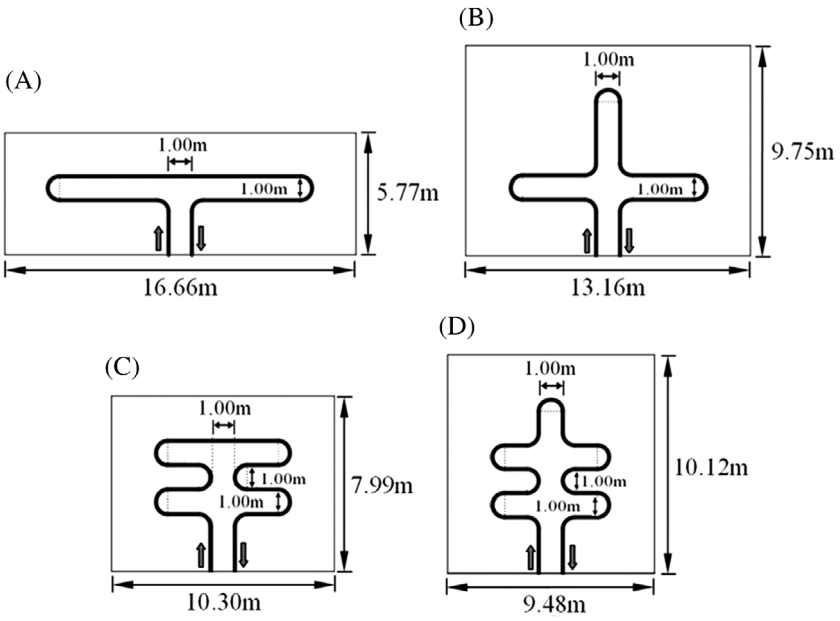

FIGURE 5 Configurations of the EAHE of the Group 3: A, Installation 11 (I11), B, Installation 12 (I12), C, Installation 13 (I13) and D, Installation 14 (I14)

installations I6, I7, I8, I9, and I10, respectively. Moreover, for cases of Group 2 it is considered $S = 1.00$ m, generating soil volumes occupations equal to 1796.76 m^3; 1501.81 m^3; 1418.57 m^3; 1449.10 m^3, and 1370.36 m^3, respectively, for I6, I7, I8, I9, and I10.

In its turn, the upper view for each EAHE installation of Group 3 is depicted in Figure 5. The spacing between parallel ducts is also $S = 1.00$ m for these cases, being the installations of Group 3 differentiated by the quantity of 90° and 180° curves needed in each arrangement. More precisely, I11 has $n = 2$ curves of 90° and $n = 2$ curves of 180°; I12 has $n = 4$ curves of 90° and $n = 3$ curves of 180°; I13 has $n = 2$ curves of 90° and $n = 6$ curves of 180° and I14 has $n = 4$ curves of 90° and $n = 7$ curves of 180°. Besides, installations I11, I12, I13, and I14 occupy soil volumes of V_s = 1441.92 m^3; 1924.65 m^3; 1234.46 m^3, and 1439.06 m^3, respectively.

The next set of scenarios, Group 4, is composed of nine arrangements (Figure 6). Installations of Group 4 has 90° and 180° curves and values for spacing between ducts S equal to 1.00 m or 2.00 m. In this way, installations are differentiated by quantity of curves and by the use of two different spacing between ducts (see Figure 6). Concerning the soil volumes, I15, I16, I17, I18, I19, I20, I21, I22, and I23 have V_s = 2041.91 m^3; 1332.59 m^3; 1260.94 m^3; 1390.51 m^3; 1.353.04 m^3, 1.418.62 m^3, 1661.55 m^3; 1449.98 m^3, and 1760.02 m^3, as can be seen in Figures 6A-I), respectively.

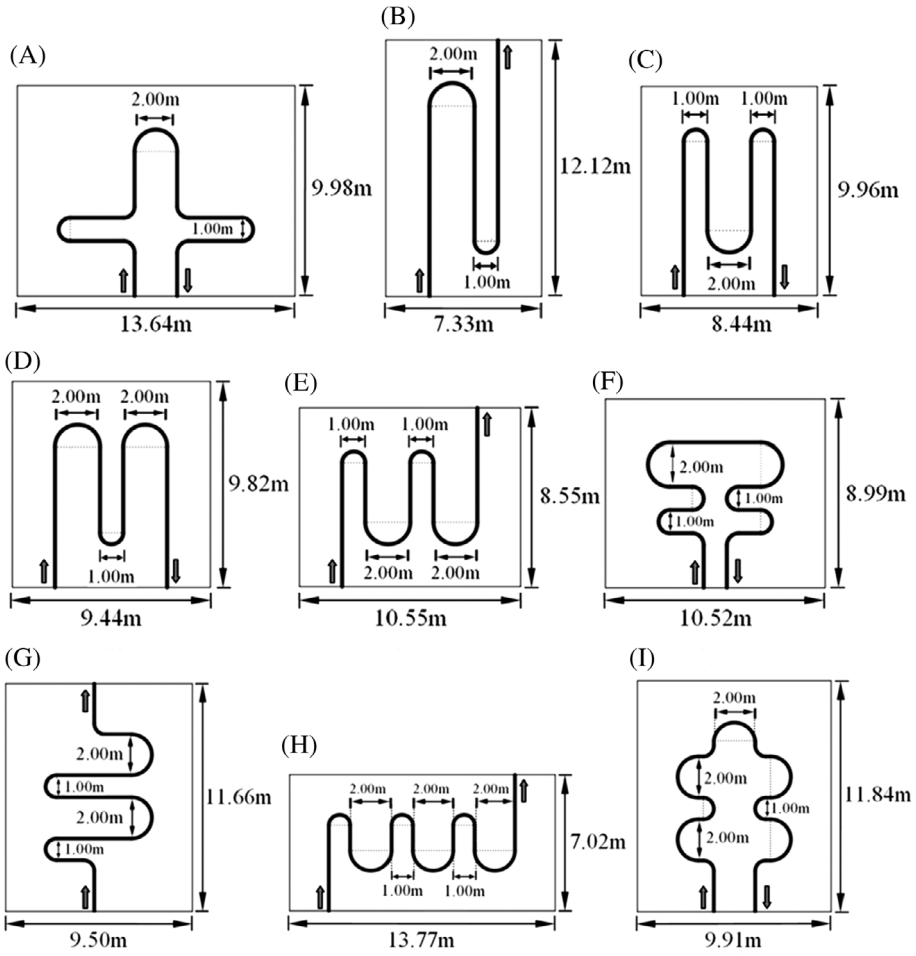

FIGURE 6 Configurations of the EAHE of the Group 4: A, Installation 15 (I15), B, Installation 16 (I16), C, Installation 17 (I17), D, Installation 18 (I18), E, Installation 19 (I19), F, Installation 20 (I20), G, Installation 21 (I21), H, Installation 22 (I22) and I, Installation 23 (I23)

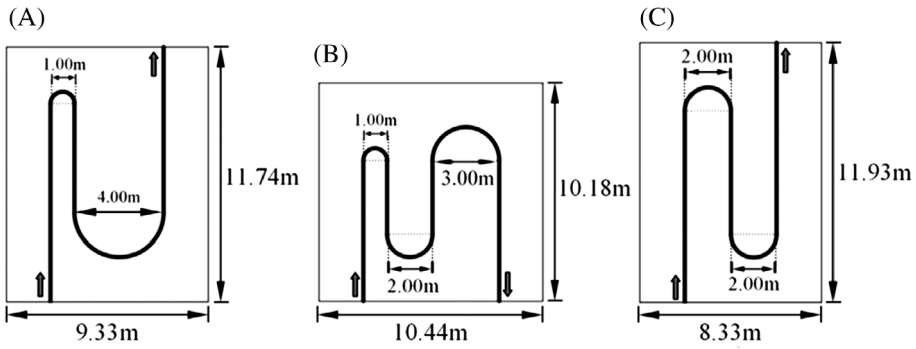

FIGURE 7 Configurations of the EAHE of the Group 5: A, Installation 24 (I24), B, Installation 25 (I25) and C, Installation 26 (I26)

Finally, Figure 7 shows the upper view of the EAHE installations of Group 5. In this group, installations have only 180° curves constructed with spacing between parallel ducts of $S = 1.00$ m; 2.00 m; 3.00 m or 4.00 m. It is possible to note that I24 has $n = 2$ curves of 180° with $S = 1.00$ m or 4.00 m. I25 contains $n = 3$ curves of 180° and $S = 1.00$ m; 2.00 m or 3.00 m, respectively. Finally, I26 has $n = 2$ curves of 180°, both with $S = 2.00$ m. From this, soil volumes of $V_s = 1643.01$ m^3; 1.594.19 m^3, and 1.490.65 m^3 have been defined for installations I24, I25, and I26, respectively.

5 | RESULTS AND DISCUSSION

Firstly, three different performance indicators have been considered in the geometric optimization here presented: the soil volume occupied by installation, the pressure drop of the airflow inside the duct and the thermal potential (*TP*) of the EAHE.

On this regard, Figure 8A shows that installations proposed in Group 1 are able to significantly reduce soil volume occupied by EAHE, indicating that the use of this kind of configuration is particularly indicated for

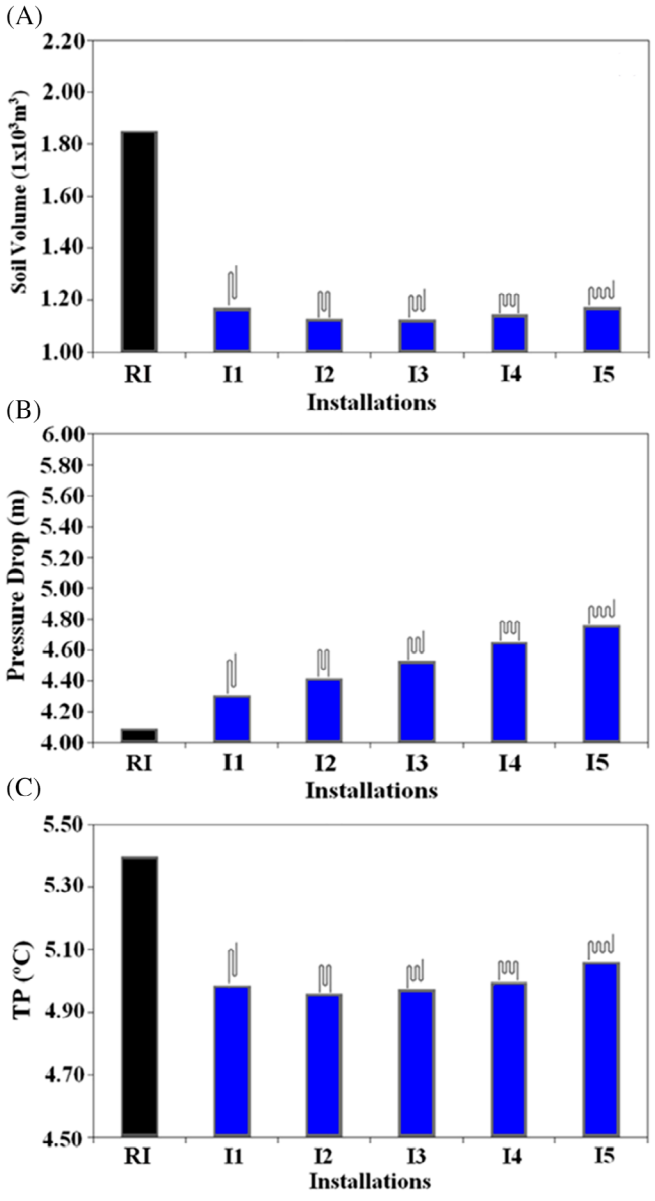

FIGURE 8 Results for EAHE installations of Group 1: A, soil volume, B, pressure drop, and C, thermal potential

application in urbanized areas, where there are more limitations of space for buildings. More specifically, it is observed that I3 obtained the lowest soil volume occupied by the EAHE in Group 1, being equal to 1.12×10^3 m^3. When the soil volume occupied by I3 is compared with the RI a reduction of nearly 39% in the soil volume is noticed.

Figure 8B shows that I1 provides the lowest air pressure drop (in meters of water column) among installations of the Group 1 being equal to 4.31 m. However, I1 presents an increase in air pressure drop equal to 5.37% in comparison with RI. As expected, I5 presents the highest air pressure drop among installations of the Group 1. This fact is due to the increase of complexity of the geometric configuration, obviously providing an increase in the pressure drop of airflow of the EAHE. Analyzing in combined way Figure 8A,B it is possible to observe a slight variation of V_s for all installations of Group 1 and a more pronounced variation in pressure drop. Regarding this specific case, the pressure drop can prevail over the volume of soil as a selection criterion for the best design of Group 1.

Figure 8C shows that the thermal behavior of the EAHE is not significantly affected by the geometrical complexity of the installations composing Group 1, being the maximum variation among the cases approximately 0.1°C. In spite of slight differences, I5 obtained the highest thermal performance in relation to the other installations of Group 1, reaching to a $TP = 5.05$°C. Therefore, *TP* of I5 is the one that most approached the *TP* of the RI ($TP = 5.40$°C). Based on pure observation, when installations of Group 1 are compared, the augmentation in the number of curves proved to enhance thermal exchange between soil and air. Consequently, results indicate that serpentine designs, similar to that found in heat exchangers, condensers, and evaporators are also essential promoters for the thermal potential in EAHE.

Regarding Group 2, Figure 9A shows that the soil volume occupied by I10 is the lowest among all installations: it corresponds to a reduction in soil volume of 25.93% when compared to the soil volume occupied by RI. On the opposite, I6 occupies the largest soil volume with a difference of only 2.81% in comparison with RI.

Still regarding Group 2, with reference to the pressure drop indicator, Figure 9B highlights similar trends already observed in Figure 8B for Group 1, that is, RI has a steep difference in comparison with complex arrangements. Moreover, the increase of complexity leads to an augmentation of pressure drop in the device, as expected. Even the best case of Group 2 (I6) led to a pressure drop 13.69% higher than that obtained for RI. As for the thermal investigation, Figure 9C depicts the thermal potential (*TP*) for arrangements of Group 2. Based on pure observation, a configuration with intermediate complexity geometry (I9) led to the best thermal potential among the cases of Group 2, with $TP = 5.18$°C. In spite of *TP* for I9 being worse than that reached for RI, it is noticed an augmentation of thermal performance in comparison with the best geometrical configuration of Group 1 (I5), as perceived in Figure 8C. The main difference for the two designs (I9 and I5) is the points of inlet and outlet of the airflow in the arrangement, which for Group 2 are aligned, while for Group 1 are misaligned.

In sequence, the installations of Group 3 are now evaluated. Figure 10A shows the influence of geometric configurations of Group 3 over the volume of soil

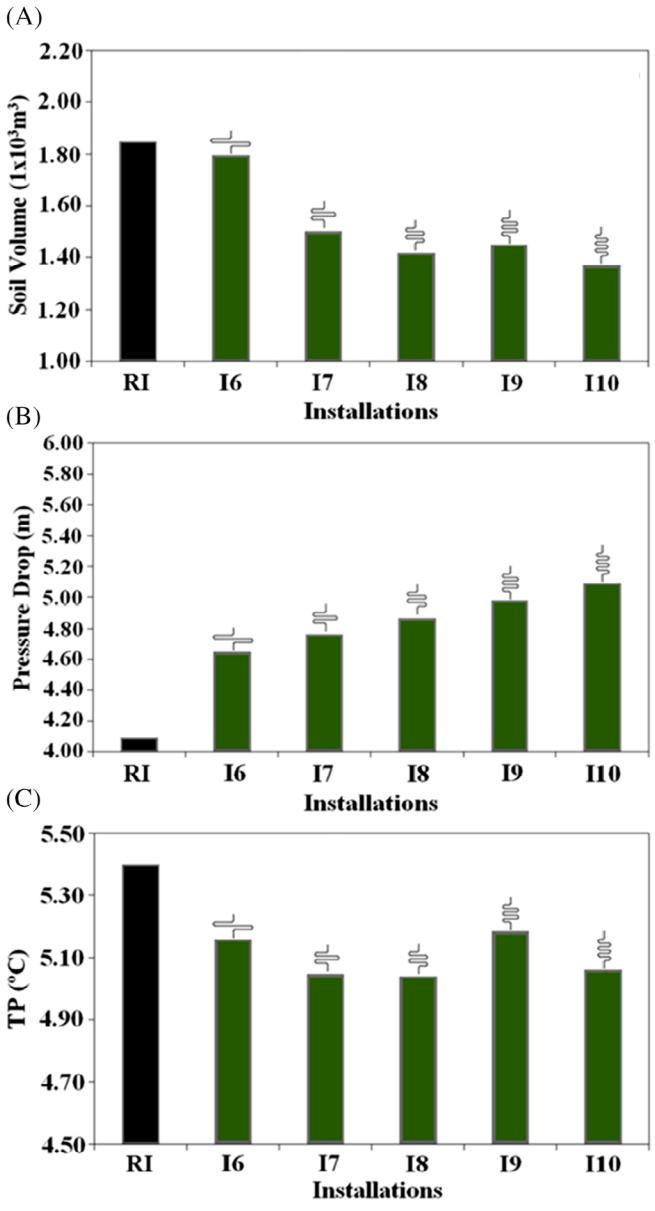

FIGURE 9 Results for EAHE installations of Group 2: A, soil volume, B, pressure drop, and C, thermal potential

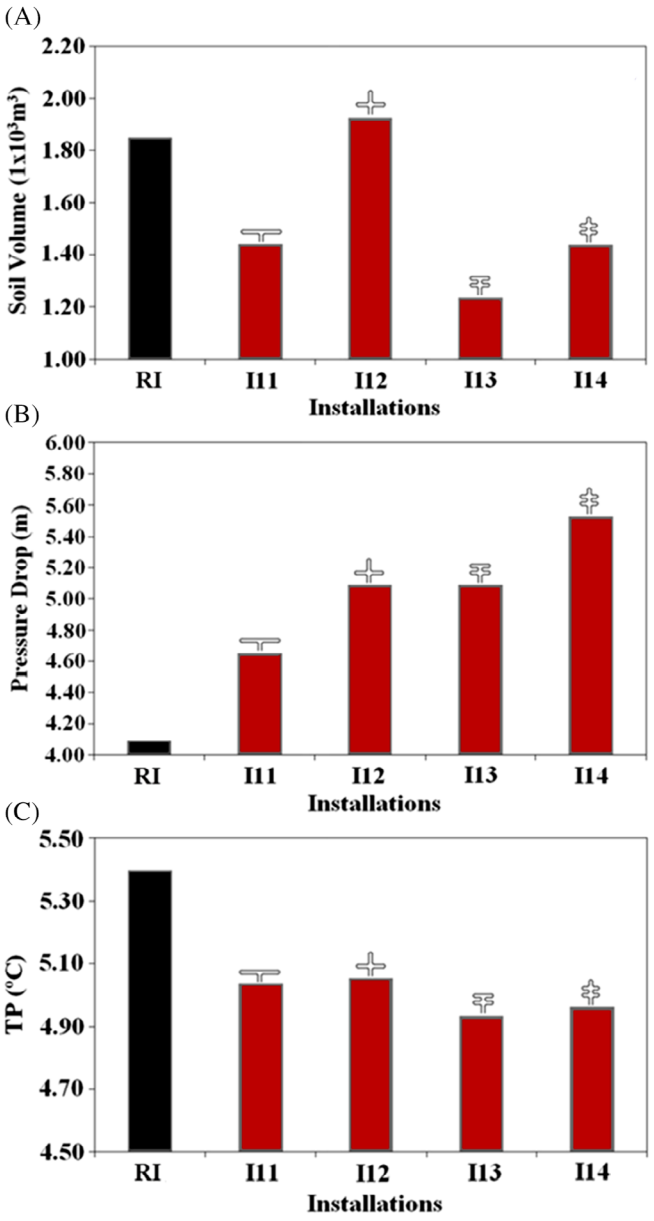

FIGURE 10 Results for EAHE installations of Group 3: A, soil volume, B, pressure drop, and C, thermal potential

occupied by the EAHE. It is observed that I12 required the largest soil volume among all installations of the Group 3, including that required for Reference Installation (RI). More specifically, soil volume occupied by I12 exceeds the soil volume occupied by RI in the order of 4.08%. Among the scenarios of Group 3, the installation I13 occupied the lowest soil volume, showing a reduction of 33.16% if compared to RI. In general, it can be perceived that the use of few curves in different directions led to high occupancy volumes for the EAHE. Therefore, this kind of arrangement is not recommended for urban applications.

As for the evaluation of pressure drop, Figure 10B shows its increase caused by the augmentation of the geometrical complexity, with reference to the installations of Group 3. Moreover, it is also observed that I12 and I13 are characterized by equivalent air pressure drop. Installation I14 presents the highest pressure drop among all installations of Group 3, with an increase equal to 35.20% in relation to RI.

Regarding the thermal potential, Figure 10C shows that there is no significant variation in the *TP* of the EAHE among the installations of Group 3. The design I12 presents the highest magnitude of *TP*, even if it is 6.37% lower than the *TP* obtained for RI. Moreover, all results of Figure 10 indicate that *TP* has not a strong sensibility to the different scenarios of Group 3 so that the

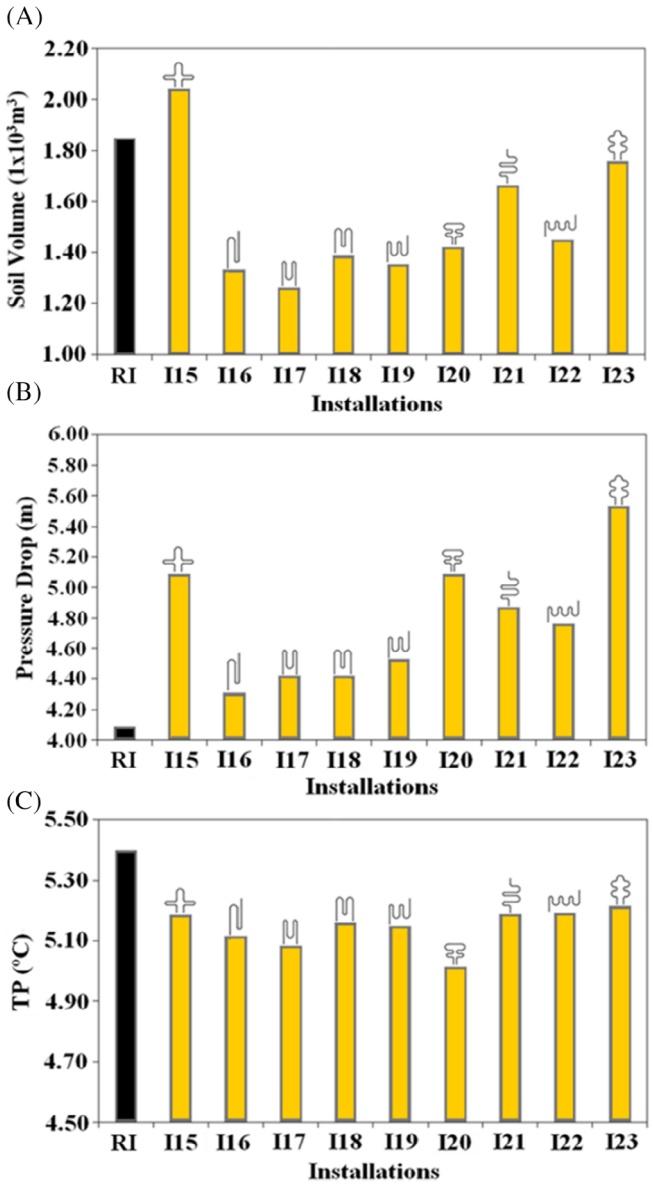

FIGURE 11 Results for EAHE installations of Group 4: A, soil volume, B, pressure drop, and C, thermal potential

choice of design tends to be governed by pressure drop and/or soil volume. In this sense, configurations I11 and I13 are the most indicated for Group 3. In spite of a good strategy for pressure drop and thermal potential, installation I12 needs a large volume occupation, which consequently restricts its use in urban applications.

As for Group 4, Figure 11A shows that configuration I15 occupies the largest soil volume, exceeding the soil volume needed to the RI in the order of 10.48%. This trend is similar to that noticed for case I12 of Group 3 (see Figure 10A). On the opposite, I17 occupies a soil volume 31.78% lower than that required for RI. A comparison between the opposite extreme configurations, that is, regarding the highest and lowest V_s, leads to a difference of around 63%.

As for the pressure drop performance indicator, Figure 11B shows that, as predictable, I23 presents the highest air pressure drop among all installations of Group 4. It is worth mentioning that the same tendency was previously observed in the air pressure drop obtained in configuration I14 (see Figure 10B). However, the design configuration I16 offers the lowest resistance to the airflow inside duct in relation to installations of Group 4. Nevertheless, I16 exceeds in 5.37%, if compared to the pressure drop of the RI.

For thermal potential indicator, Figure 11C indicates that *TP* of I23 is the largest among installations of Group 4 being equal to 5.2°C, being *TP* of the RI equal to 5.4°C. In addition, a maximum variation of 0.21°C is identified between I23 and I20, since I20 provides the lowest *TP* of the EAHE among all the installations of Group 4. In general, the results for thermal potential of Group 4 reveal that the employment of different spacings reduces the difference of thermal performance between the simplest and most complex designs. It is also noticed that the variations in thermal potential do not seem more intensive than variations in the pressure drop and occupation of volume of soil.

Regarding the evaluation of Group 5 performance, Figure 12A shows the required soil volume for installations I24, I25, and I26. Results indicate that all proposed geometries in Group 5 led to a V_s lower than that reached for RI configuration, being the installation I26 the one which needs the lowest soil volume. More specifically, the soil volume occupied by the I26 is 19.34% lower than the RI configuration.

For the pressure drop analysis of Group 5, Figure 12B identifies again that the simplest configuration conducts to the best fluid dynamic performance, minimizing the pressure drop in the ducts. Results also demonstrated the possibility to design EAHE configurations that provide an air pressure drop with an increase of only 5.37% if compared with the RI geometry, as those noticed for I24 and I26.

As for thermal potential indicator, Figure 12C reveals that there is no significant variation among the *TP* for all installations of Group 5.

Therefore, regarding all proposed complex geometries for the EAHE, it is possible to demonstrate that most of these installations can promote a reduction in soil volume occupied by the EAHE, if compared with RI (see Figure 8A-12A). Moreover, it can be observed that all the studied configurations of EAHE are not able to offer a reduction in the air pressure drop in the ducts in comparison to air pressure drop of the RI, which is consistent since all the proposed designs have more complex

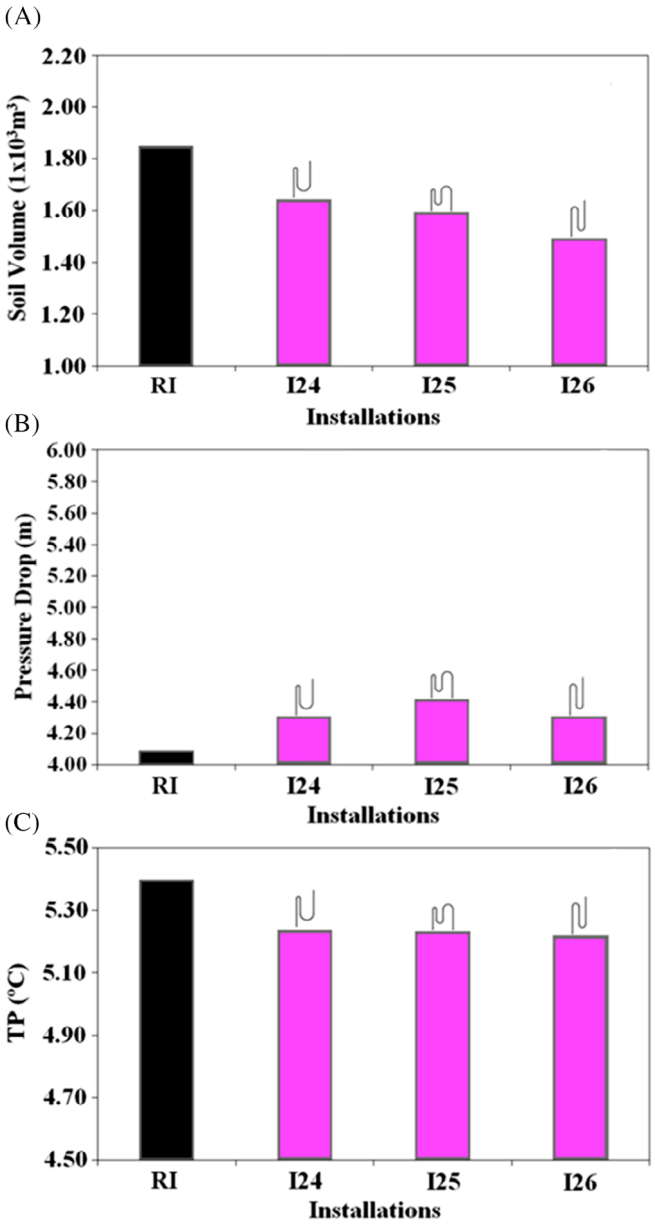

FIGURE 12 Results for EAHE installations of Group 5: A, soil volume, B, pressure drop, and C, thermal potential

geometry. However, it is possible to recommend some installations with low resistance to airflow and important reduction of soil volume occupation (see Figures 8B-12B). Moreover, the results of the *TP* of the EAHE indicate that all the studied arrangements are not able to provide an increase in *TP* in comparison to the one reached by RI. Nevertheless, it is possible to identify EAHE designs with a performance similar to that achieved for RI with a lower soil volume occupation (see Figures 8C-12c).

Finally, aiming to perform a global multi-objective analysis, the normalized performance indicators - soil volume occupied by the EAHE (V_N), air pressure drop (h_N), and thermal potential ($(TP_N)^{-1}$) - are evaluated concomitantly (see Equations [4], [10], and [12], respectively). Therefore, the minimization of these performance indicators is associated with a better overall performance among the EAHE installations here pointed out. For this purpose, a vector magnitude of imperfection has been introduced and calculated by the distance between the point with coordinates (V_N, h_N, $(TP_N)^{-1}$) of each proposed installation and an ideal hypothetical case (that would be an EAHE with $V_N = h_N = (TP_N)^{-1} = 0$). Evidently, the design which leads to the lowest distance is considered the best configuration from the multi-objective viewpoint. It is worth mentioning that, in the present work, no weighting factors are used to correlate the three above-mentioned different indicators. However, depending on the costs concerned with the build and maintenance of the device or the need to prioritize one determined performance indicator, a sort of ponderation can be all the same used in the treatment. That said, this final analysis gives an idea about the particular performance of each installation in the multi-objective viewpoint, allowing a global comparison among all EAHE complex geometries. Figure 13 displays the vector magnitude of each EAHE complex geometric configuration related to the ideal hypothetical EAHE. In addition, Figure 13 also indicates the vector magnitude of the Reference Installation (RI).

Based on pure observation, Figure 13 highlights that installations of Group 1 present in general smaller magnitudes of distance between multi-objective performance indicator and ideal hypothetical EAHE in comparison with the other scenarios. In addition, it can be observed that Groups 3 and 4 include the cases with highest magnitudes in comparison with other groups. More specifically, the smallest magnitude is reached for the design I1 with the value of 1.64, while the largest vector magnitude is obtained for installation I15 with the value of 1.96. Consequently, it is possible to affirm that I1 has a global performance 16.33% superior than I15 in the context of multi-objective analysis.

Moreover, still considering Figure 13 and regarding the conventional EAHE with straight duct adopted as reference, one can note that several of the proposed complex EAHE installations achieve an overall performance better than the RI, that is, they have a vector magnitude inferior than RI. For instance, the design I1 (with vector magnitude of 1.64) allows a global improvement of 5.20% if compared with the RI (that has a vector magnitude of 1.73).

In summary, for the multi-objective analysis and considering the conditions defined here, the best EAHE configurations are those with the lowest possible V_N and h_N and with intermediate magnitudes of TP_N (I1 and I2). On the opposite, the worst configurations are those with

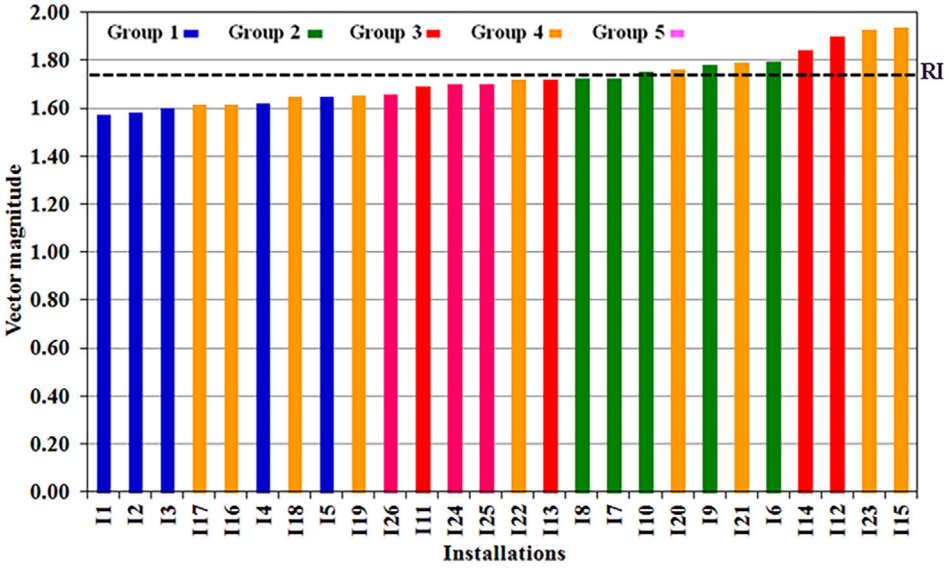

FIGURE 13 Module of the distance between performance indicator coordinate and an ideal hypothetical EAHE with $V_N = h_N = (TP_N)^{-1} = 0$

poor performance for minimize the volume occupied by the soil and pressure drop (I15 and I23). The dispersion of thermal potential is lower here and the best designs for *TP* are only classified in intermediate positions, for example, I5 and I9, in the multi-objective evaluation.

6 | CONCLUSIONS

In the present analytical and numerical work, EAHE installations with several different complex configurations were proposed, aiming to perform a comparative analysis among these designs, in coherence with Constructal Design. More specifically, 26 different geometrical configurations were analyzed seeking to minimize the soil volume occupied by the EAHE arrangement, minimize its airflow pressure drop and maximize its thermal potential. An EAHE with straight duct, having diameter and length constant, has been considered as Reference Installation (RI) for the proposition and comparison of all complex EAHE arrangements. Hence, the same overall volume of duct airflow was imposed for all analyzed cases, being this the main problem constraint. Many ideas emerged from this work for the design of EAHE in urban areas. This kind of recommendation with the application of Constructal Design for the complex configurations proposed here was not previously investigated in the literature.

Results revealed that the best recommended configurations are dependent of the performance indicator that dominates the design of the EAHE. The RI was the best configuration to maximize the thermal performance and minimize the pressure drop. However, this configuration required large space for its setting up, which can be an important limitation for its application in urban areas.

Concerning the evaluation of soil volume occupied by the EAHE installation, it was demonstrated that several configurations in serpentine arrangement conducted to a robust reduction in the volume needed for the device. The configurations I3, I10, I13, I17, and I26 were the best for each group to minimize the volume of soil necessary to install the EAHE. In general, these arrangements had multiple curves, being this strategy recommended for design of the EAHE in urban areas. In addition, the best configuration (I3) allowed a reduction of nearly 39% in the soil volume compared with the RI.

As for the pressure drop performance indicator, it was noticed that the best configurations were achieved for installations I1, I6, I11, I16, and I26. As expected, the results demonstrated that, within the configurations here investigated, the minimization of pressure drop is reached for the simplest designs, that is, the ones having few curves. The best configurations (I1, I16, and I26) performed nearly 30% better than the worst configurations (I14 and I23).

Regarding thermal purpose, there was no significant variation on thermal potential in the different arrangements. The best installations found for each group proved to be I5, I9, I12, I23, and I24. In a general way, these configurations were the most complex possible, that is, the ones with curves and lines distributed in different directions. For this performance indicator, it was recommended the most complex possible configuration, with multiple curves. The best configurations were slight better than the worst ones, with differences of almost 6%.

Into the multi-objective viewpoint, the arrangements I1, I2, and I16 were the three best configurations, that is, the ones which minimized the vector magnitude representing the distance between the point composed by V_N, h_N, and $(TP_N)^{-1}$ with the point zero of an ideal hypothetical EAHE. In addition to these three designs, several other proposed EAHE configurations also presented an overall performance superior than the RI. This is an important finding addressed to the use of EAHE in urban areas. For instance, the configuration I1 has an overall performance 5.20% superior than the RI, due to a reduction of 36.75% in the occupied soil volume, an increase of 5.37% in air pressure drop, and a decrease of 7.96% in *TP* of EAHE in relation to RI. Furthermore, despite the slight worsening of pressure drop and thermal potential, the design I1 can be considered as a promising geometric arrangement of an EAHE to be installed in urban regions, because of the significant reduction in the occupied soil for the EAHE installation.

As future developments of the present work, we are certain that Constructal Design method may be hopefully used with reference to the optimization of EAHE geometries, taking into account additional performance indicators, such as those related with cost analysis.

ACKNOWLEDGEMENTS

The authors thank the CAPES-COFECUB program (Ph 854-15) at the origin of this work. E.D. Dos Santos and L.A.O. Rocha's visits in Toulouse were funded by CAPES, Brazil. EElizaldo Domingues dos Santos, Liércio André Isoldi, and Luiz Alberto Oliveira Rocha thank CNPq (Brasília, DF, Brazil) for research grants (Processes: 306024/2017-9, 306012/2017-0, 307791/2019-0). The authors also thank to FAPERGS by the financial support (*Edital* 02/2017 - PqG - Process: 17/2551-0001111-2). The author Cesare Biserni was sponsored by the Italian Ministry for Education, University and Research. Open Access Funding provided by Universita di Bologna within the CRUI-CARE Agreement.

ORCID

Matthieu Labat https://orcid.org/0000-0003-4532-4327
Cesare Biserni https://orcid.org/0000-0003-0081-2036

REFERENCES

1. Rodrigues MK, Brum RS, Vaz J, Rocha LAO, Dos Santos ED, Isoldi LA. Numerical investigation about the improvement of the thermal potential of an earth-air heat exchanger (EAHE) employing the constructal design method. *Renew Energy*. 2015;80:538-551. https://doi.org/10.1016/j.renene.2015.02.041
2. Bordoloi N, Sharma A, Nautival H, Goel V. An intense review on the latest advancements of earth air heat exchangers. *Renew Sust Energ Rev*. 2018;89:261-280. https://doi.org/10.1016/j.rser.2018.03.056
3. Bharadwaj S, Bansal N. Temperature distribution inside ground for various surface conditions. *Build Environ*. 1981;16:183-192. https://doi.org/10.1016/0360-1323(81)90012-3
4. Givoni B, Katz L. Earth temperatures and underground buildings. *Energ Buildings*. 1985;8:15-25. https://doi.org/10.1016/0378-7788(85)90011-8
5. Mihalakakou G, Santamoures M, Asimakopoulos DN, Argiriou A. On the ground temperature below buildings. *Sol Energy*. 1995;55(5):355-362. https://doi.org/10.1016/0038-092X(95)00060-5
6. Jacovides CP, Mihalakakou G, Santamoures M, Lewis JO. On the ground temperature profile for passive cooling applications in buildings. *Sol Energy*. 1996;57(3):167-175. https://doi.org/10.1016/S0038-092X(96)00072-2
7. Mihalakakou G, Santamoures M, Lewis JO, Asimakopoulos DN. On the application of the energy balance equation to predict ground temperature profiles. *Sol Energy*. 1997;60(3–4):181-190. https://doi.org/10.1016/S0038-092X(97)00012-1
8. Serageldin AA, Abdelrahman AK, Ookawara S. Earth-air heat exchanger thermal performance in Egyptian conditions: experimental results, mathematical model, and computational fluid dynamics simulation. *Energy Convers Manag*. 2016;122:25-38. https://doi.org/10.1016/j.enconman.2016.05.053
9. Yang D, Guo Y, Zhang J. Evaluation of the thermal performance of an earth-to-air heat exchanger (EAHE) in a harmonic thermal environment. *Energy Convers Manag*. 2016;109:184-194. https://doi.org/10.1016/j.enconman.2015.11.050
10. Wei H, Yang D, Wang J, Du J. Field experiments on the cooling capability of earth-to-air heat exchangers in hot and humid climate. *Appl Energy*. 2020;276:115493. https://doi.org/10.1016/j.apenergy.2020.115493
11. Vaz J, Sattler MA, Dos Santos ED, Isoldi LA. Experimental and numerical analysis of an earth–air heat exchanger. *Energ Buildings*. 2011;43:2476-2482. https://doi.org/10.1016/j.enbuild.2011.06.003
12. Brum RS, Vaz J, Rocha LAO, Dos Santos ED, Isoldi LA. A new computational modeling to predict the behavior of earth-air heat exchangers. *Energ Buildings*. 2013;64:395-402. https://doi.org/10.1016/j.enbuild.2013.05.032
13. Bansal V, Misra R, Agarwal GD, Mathur J. Transient effect of soil thermal conductivity and duration of operation on performance of earth air tunnel heat exchanger. *Appl Energy*. 2013;103:1-11. https://doi.org/10.1016/j.apenergy.2012.10.014
14. Cuny M, Lin J, Siroux M, Magnenet V, Fond C. Influence of coating soil types on the energy of earth-air heat exchanger. *Energ Buildings*. 2018;158:1000-1012. https://doi.org/10.1016/j.enbuild.2017.10.048
15. Menhoudi S, Mokhtari A-M, Benzaama M-H, Maalouf C, Lachic M, Makhlouf M. Study of the energy performance of an earth-air heat exchanger for refreshing buildings in Algeria. *Energ Buildings*. 2018;158:1602-1612. https://doi.org/10.1016/j.enbuild.2017.11.056
16. Rocha LAO, Lorente S, Bejan A, Anderson R. Constructal design of underground heat sources or sinks for the annual cycle. *Int J Heat Mass Transf*. 2012;55:7832-7837. https://doi.org/10.1016/j.ijheatmasstransfer.2012.08.010

17. Mathur A, Priyam A, Mathur S, Agrawal GD, Mathur J. Comparative study of straight and spiral earth air tunnel heat exchanger system operated in cooling and heating modes. *Renew Energy*. 2017;108:474-487. https://doi.org/10.1016/j.renene.2017.03.001
18. Fazlikhani F, Goudarzi H, Solgi E. Numerical analysis of the efficiency of earth to air heat exchange Systems in cold and hot-arid climates. *Energy Convers Manag*. 2017;148:78-89. https://doi.org/10.1016/j.enconman.2017.05.069
19. Shojaee SMN, Malek K. Earth-to-air heat exchangers cooling evaluation for different climates of Iran. *Sustain Energy Technol*. 2017;23:111-120. https://doi.org/10.1016/j.seta.2017.09.007
20. Rosa N, Soares N, Costa JJ, Gervásio H. Assessment of an earth-air heat exchanger (EAHE) system for residential buildings in warm-summer Mediterranean climate. *Sustain Energy Technol*. 2020;38:100649. https://doi.org/10.1016/j.seta.2020.100649
21. Elminshawy NAS, Siddiqui FR, Farooq QU, Addas MF. Experimental investigation on the performance of earth-air pipe heat exchanger for different soil compaction levels. *Appl Therm Eng*. 2017;124:1319-1327. https://doi.org/10.1016/j.applthermaleng.2017.06.119
22. Uddin S, Ahmed R, Rahman M. Performance evaluation and life cycle analysis of earth to air heat exchanger in a developing country. *Energ Buildings*. 2016;128:254-261. https://doi.org/10.1016/j.enbuild.2016.06.088
23. Bisoniya TS, Kumar A, Baredar P. Energy metrics of earth-air heat exchanger system for hot and dry climatic conditions of India. *Energ Buildings*. 2015;86:214-221. https://doi.org/10.1016/j.enbuild.2014.10.012
24. Victoria LC, Hermes VF, Vaz J, et al. Methodology allying standard penetration test and era-interim data set for numerical simulations of earth-air heat exchangers. *J Adv Res Fluid Mech Therm Sci*. 2020;76(2):43-64. https://doi.org/10.37934/arfmts.76.2.4364
25. Hermes VF, Ramalho JVA, Rocha LAO, et al. Further realistic annual simulations of earth-air heat exchangers installations in a Coastal city. *Sustain Energy Technol*. 2020;37:100603. https://doi.org/10.1016/j.seta.2019.100603
26. Paludetto D, Lorente S. Modeling the heat exchanges between a datacenter and neighboring buildings through an underground loop. *Renew Energy*. 2016;93:502-509. https://doi.org/10.1016/j.renene.2016.02.081
27. Brum RS, Ramalho JVA, Rodrigues MK, Rocha LAO, Isoldi LA, Dos Santos ED. Design evaluation of earth-air heat exchangers with multiple ducts. *Renew Energy*. 2019;135:1371-1385. https://doi.org/10.1016/j.renene.2018.09.063
28. Bejan A. *Shape and Structure from Engineering to Nature*. New York: Cambridge University Press; 2000.
29. Bejan A, Lorente S. *Design with Constructal Theory*. Hoboken: John Wiley & Sons; 2008.
30. Bejan A, Zane P. *Design in Nature: how the Constructal Law Governs Evolution in Biology, Physics, Technology, and Social Organization*. First ed. New York: Doubleday; 2012.
31. Bejan A. *The Physics of Life: the Evolution of Everything*. New York: St. Martins Press; 2016.
32. Bejan A. Evolution in thermodynamics. *Appl Phys Rev*. 2017;4:011305. https://doi.org/10.1063/1.4978611
33. Teixeira FB, Lorenzini G, Errera MR, Rocha LAO, Isoldi LA, Dos Santos ED. Constructal design of triangular arrangements of square bluff bodies under forced convective turbulent flows. *Int J Heat Mass Transf*. 2018;126:521-535. https://doi.org/10.1016/j.ijheatmasstransfer.2018.04.134
34. Estrada ESD, Labat M, Lorente S, Rocha LAO. The impact of latent heat exchanges on the design of earth air heat exchangers. *Appl Therm Eng*. 2018;129:306-317. https://doi.org/10.1016/j.applthermaleng.2017.10.007
35. Lima JPS, Cunha ML, Dos Santos ED, Rocha LAO, Real MV, Isoldi LA. Constructal design for the ultimate buckling stress improvement of stiffened plates submitted to uniaxial compressive load. *Eng Struct*. 2020;203:109883–109883-16. https://doi.org/10.1016/j.engstruct.2019.109883
36. Florides G, Kalogirou S. Ground heat exchangers: a review of systems, models and applications. *Renew Energy*. 2007;32:2461-2478. https://doi.org/10.1016/j.renene.2006.12.014
37. Bisoniya TS, Kumar A, Baredar PE. Experimental and analytical studies of earth-air heat exchanger (EAHE) systems in India. A review. *Renew Sustain Energy Rev*. 2013;19:238-246. https://doi.org/10.1016/j.rser.2012.11.023
38. Peretti C, Zarrella A, Carli M, Zecchin R. The design and environmental evaluation of earth-to-air heat exchangers (EAHE): a literature review. *Renew Sust Energ Rev*. 2013;28:107-116. https://doi.org/10.1016/j.rser.2013.07.057
39. Sobti J, Singh SK. Earth-air heat exchanger as a green retrofit for Chandīgarh - a critical review. *Geotherm Energy*. 2015;9:1-9. https://doi.org/10.1186/s40517-015-0034-4
40. Ozgener O, Ozgener L, Goswami DY. Experimental prediction of total thermal resistance of a closed loop EAHE for greenhouse cooling system. *Int Commun Heat Mass Transfer*. 2011;38:711-716. https://doi.org/10.1016/j.icheatmasstransfer.2011.03.009
41. Verma MK, Bansal V, Rana KB. Development of passive energy source as earth air pipe heat exchangers (EAPHE) system - a review. *J Therm Eng*. 2020;6(5):651-676. https://doi.org/10.18186/thermal.790173
42. Bansal V, Misra R, Agrawal GD, Mathur J. Performance analysis of earty-pipeair heat exchanger for winter heating. *Energ Buildings*. 2009;41:1151-1154. https://doi.org/10.1016/j.enbuild.2009.05.010
43. Bansal V, Misra R, Agrawal GD, Mathur J. Performance analysis of earty-pipeair heat exchanger for summer cooling. *Energ Buildings*. 2010;42:645-648. https://doi.org/10.1016/j.enbuild.2009.11.001
44. Marzarotto C, Nunes B, Rodrigues MK, et al. Numerical analysis of the influence of operational and constructive parameters on the operation of earth-air heat exchangers (*in Portuguese*). *Sci Plena*. 2015;11:1-10. https://doi.org/10.14808/sci.plena.2015.081304
45. Pritchard PJ, Mitchell JW. *Fox and McDonald's: Introduction to Fluid Mechanics*. 9th ed. Hoboken: John Wiley & Sons Inc.; 2015.
46. White FM. *Viscous Fluid Flow*. 3rd ed. New York: McGraw-Hill; 2006.
47. Haaland SE. Simple and explicit formulas for the friction factor in turbulent flow. *J Fluids Eng*. 1983;103:89-90. https://doi.org/10.1115/1.3240948
48. Versteeg H, Malalasekera W. *An Introduction to Computational Fluid Dynamics: the Finite Volume Method*. England: Pearson Education Limited; 2007.
49. Patankar S. *Numerical Heat Transfer and Fluid Flow*. New York: McGraw-Hill; 1980.

50. ANSYS. 14.0. – FLUENT User's Guide, ANSYS Inc. 2011.
51. Bejan A. *Convection Heat Transfer*. 4th ed. Hoboken: John Wiley & Sons Inc.; 2013.
52. Bejan A, Kraus AD. *Heat Transfer Handbook*. Hoboken: John Wiley & Sons Inc.; 2003.
53. Wilcox DC. *Turbulence Modeling for CFD*. California: DCW Industries; 2002.
54. Launder BE, Salding DB. *Lectures in Mathematical Models of Turbulence*. London: Academic Press; 1972.

How to cite this article: Nunes BR, Rodrigues MK, Oliveira Rocha LA, et al. Numerical-analytical study of earth-air heat exchangers with complex geometries guided by constructal design. *Int J Energy Res*. 2021;45(15): 20970-20987. https://doi.org/10.1002/er.7157